

## A CEPHEID DISTANCE TO NGC 4603 IN CENTAURUS

JEFFREY A. NEWMAN<sup>1</sup>, STEPHEN E. ZEPF<sup>2</sup>, MARC DAVIS<sup>1</sup>, WENDY L. FREEDMAN<sup>3</sup>, BARRY F. MADORE<sup>4</sup>,PETER B. STETSON<sup>5</sup>, N. SILBERMANN<sup>6</sup>, AND RANDY PHELPS<sup>3</sup>

e-mail: jnewman@astro.berkeley.edu, zepf@astro.yale.edu, marc@astro.berkeley.edu, wendy@ociw.edu, barry@ipac.caltech.edu, Peter.Stetson@hia.nrc.ca, nancys@ipac.caltech.edu, rphelps@physics.oberlin.edu

*Ap. J., accepted*

## ABSTRACT

In an attempt to use Cepheid variables to determine the distance to the Centaurus cluster, we have obtained images of NGC 4603 with the Hubble Space Telescope for 9 epochs (totalling 24 orbits) over 14 months in the F555W filter and 2 epochs (totalling 6 orbits) in the F814W filter. This galaxy has been suggested to lie within the “Cen30” portion of the Centaurus cluster, which is concentrated around a heliocentric redshift of  $\approx 3000 \text{ km s}^{-1}$ , and is the most distant object for which this method has been attempted. Previous distance estimates for Cen30 have varied significantly and some have presented disagreements with the peculiar velocity predicted on the basis of full-sky redshift surveys of galaxies, motivating our investigation. Using our WFPC2 observations, we have found 61 candidate Cepheid variable stars with well-determined oscillation periods and mean magnitudes; however, a significant fraction of these candidates are likely to be nonvariable stars whose magnitude measurement errors happen to fit a Cepheid light curve of significant amplitude for some choice of period and phase. Through a maximum likelihood technique, we determine that we have observed  $43 \pm 7$  real Cepheids (with zero excluded at  $> 9\sigma$ ) and that NGC 4603 has a distance modulus of  $32.61^{+0.11}_{-0.10}$  (random,  $1 \sigma$ )  $^{+0.24}_{-0.25}$  (systematic, adding in quadrature), corresponding to a distance of  $33.3^{+1.7}_{-1.5}$  (random,  $1 \sigma$ )  $^{+3.8}_{-3.7}$  (systematic) Mpc. This result is consistent with a number of recent estimates of the distance to NGC 4603 or Cen30 and implies a small peculiar velocity consistent with predictions from the *IRAS* 1.2 Jy redshift survey if the galaxy lies in the foreground of the cluster.

*Subject headings:* Cepheids — galaxies: distances and redshifts — galaxies: individual (NGC 4603) — galaxies: clusters: individual (Centaurus) — cosmology: large-scale structure of universe

## 1. INTRODUCTION

The gravitational field of the inhomogeneous distribution of mass in the Universe produces observable deviations from the smooth Hubble expansion. Well-determined distances to galaxies provide an opportunity to measure their motions relative to the “Hubble flow” – so-called peculiar velocities – which can lead to mass estimates for a variety of systems, as in studies of the Local Group and of the Virgo-centric infall, or on larger scales via comparisons of peculiar velocity measurements to expectations from full-sky redshift surveys (Dekel 1994, Willick & Strauss 1995).

In such analyses, the Centaurus region is probably the most perplexing zone of large-scale flow in our vicinity. It has a complex spatial structure, and its peculiar velocity has been measured in some studies to be much higher than that expected from the observed galaxy density. Lucey, Currie, and Dickens (1986b) first called attention to the

apparently bimodal nature of the Centaurus cluster at  $(l, b) = (302^\circ, 22^\circ)$ , dividing it into two pieces at apparent redshifts in the Local Group (LG) reference frame of approximately 2800 and 4300  $\text{km s}^{-1}$  (Cen30 and Cen45, respectively). In a deeper study of the central portions of the cluster, Stein et al. (1997) found that dwarf galaxies in Centaurus exhibit a clear concentration around the redshift of NGC 4696 (an elliptical galaxy which is the brightest in the cluster),  $v_{lg} = 2674 \pm 26 \text{ km s}^{-1}$ , tracing a galaxy cluster of velocity dispersion  $933 \pm 118 \text{ km s}^{-1}$  that they identify with Cen30. Cen45, they determined, more strongly resembles a group falling into Cen30, with a small velocity dispersion ( $131 \pm 43 \text{ km s}^{-1}$ ) and a population dominated by late-type galaxies.

A number of secondary distance indicators have by now been applied to Centaurus galaxies, with often contradictory results. Aaronson *et al.* (1989) were the first to obtain distances for Centaurus spiral galaxies; they measured pe-

<sup>1</sup>Department of Astronomy, University of California, Berkeley, CA 94720<sup>2</sup>Department of Astronomy, P.O. Box 208101, Yale University, New Haven, CT 06520<sup>3</sup>Observatories of the Carnegie Institute of Washington, 813 Santa Barbara St., Pasadena, CA 91101<sup>4</sup>NASA/IPAC Extragalactic Database, Infrared Processing and Analysis Center, Jet Propulsion Laboratory, California Institute of Technology, MS 100-22, Pasadena, CA 91125<sup>5</sup>Dominion Astrophysical Observatory, 5071 W. Saanich Rd., Victoria, B.C., Canada V8X 4M6<sup>6</sup>Jet Propulsion Laboratory, California Institute of Technology, MS 100-22, Pasadena, CA 91125

cular velocities of  $-80 \pm 250$  and  $+10 \pm 450$  in the Local Group reference frame for Cen30 and Cen45, respectively. However, obtaining Tully-Fisher distances to these clusters is somewhat problematic. Because of the large velocity dispersion of Cen30 and the relatively small number of galaxies in Cen45, separating cluster from background spirals is very difficult (see Lucey, Currie and Dickens 1986a and Giovanelli et al. 1997 for examples). Reflecting these difficulties, Aaronson et al. identify 6 galaxies spanning nearly 2 magnitudes in distance modulus as belonging to Cen45. In contrast, based on  $D_n - \sigma$  observations of elliptical galaxies, Faber et al. (1989) reported the peculiar velocities for Cen30 and Cen45 to be  $+527 \pm 214$  km s $^{-1}$  and  $+1090 \pm 336$  km s $^{-1}$  in the Local Group frame.

In an attempt to resolve such contradictory estimates of the distance to the Centaurus region, we have undertaken a search for Cepheids in the spiral galaxy NGC 4603 to firmly establish its location. This galaxy is located near the center of the Cen30 cluster in position on the sky, and has a velocity  $v_{lq} = 2321 \pm 20$  km s $^{-1}$  (Willick et al.), well within the velocity dispersion of the cluster. NGC 4603 has an inclination of  $53^\circ$  and a 21cm width (20%) of 411 km s $^{-1}$  with isophotal ( $D_{25}$ ) diameter of 1.6'; Aaronson et al. (1989) show that it fits onto their IRTF relation for Cen30 galaxies quite well, with a distance modulus within 0.07 magnitudes ( $0.3\sigma$ ) of that derived for the cluster. It thus seems an appropriate choice for such a study. Such a study should also allow tests of the validity of the uniformity of the Tully-Fisher or  $D_n - \sigma$  relationships to a greater distance than has been possible before.

However, even the smaller estimates of the distance to Cen30 place it substantially further than any galaxy for which a search for Cepheids has been previously attempted, even using the Hubble Space Telescope; the greatest distance modulus previously measured with this method is that to NGC 4639,  $32.03 \pm 0.22$  ( $25.5 \pm 2.5$  Mpc; Saha et al. 1997). The redshift of Cen30 is roughly twice that of the Virgo or Fornax clusters. It is thus reasonable to expect that observing Cepheids in NGC 4603 should be difficult; not only do more distant Cepheids appear fainter, but also the crowding of stars that complicates photometry becomes more severe as the angular size distance increases. Furthermore, the Centaurus cluster lies behind a zone of substantial ( $A_V \sim 0.5$ ) Galactic extinction, making any stars observed that much fainter. In this regime, photometric errors are significant enough that nonvariable stars have an appreciable probability of appearing to vary in a manner indistinguishable from a Cepheid with significant amplitude. Such obstacles might be overcome by observing at many more epochs or with a greater exposure time per epoch than in prior Cepheid studies, but the limited availability of HST makes that infeasible.

Therefore, we have developed new techniques for dealing with such a dataset. Instead of relying on a set of variability criteria for preselection, we attempt to fit template Cepheid light curves to all stars with well-determined photometry and then apply a series of criteria that are effective at eliminating nonvariables. Even that technique leaves a substantially contaminated list of candidate Cepheids. We therefore do not obtain distance moduli from a direct Period-Luminosity relation fit, but rather have developed a Maximum Likelihood formulation that accounts for the properties of nonvariables that mimic Cepheids and of the

probability of selecting an actual Cepheid of given properties based upon the results of realistic simulations. These techniques allow us to minimize the biases in distance determination that might otherwise appear and which may have affected other Cepheid studies that have pushed the limits of the technique.

We describe the details of the observations in § 2, the procedures used to analyze the data and find Cepheids and our simulations thereof in § 3, and our Maximum Likelihood formalism and the determination of the distance to NGC 4603 in § 4.

## 2. OBSERVATIONS

We have observed NGC 4603 using the Wide Field and Planetary Camera 2 (WFPC2) instrument on the Hubble Space Telescope (HST). HST made a total of 11 distinct visits to the targeted field: 9, totaling 24 orbits, using the F555W filter (roughly equivalent to Johnson  $V$ ), and 2, totaling 6 orbits, using the F814W filter (similar to Kron-Cousins  $I$ ). To ensure ease of data analysis, the same orientation was maintained for all observations; the telescope was generally dithered by 5.5 planetary camera pixels ( $\approx 0''.25$ ) between orbits. Two successive frames of data were obtained during each orbit to minimize the effects of cosmic rays. Due to technical limitations (such as the time required to acquire the target field and the limited visibility of NGC 4603 during the course of an orbit), the total integration time was 900-1300 seconds per frame.

Our observing strategy was in general similar to that used for the  $H_0$  Key project (see, e.g., Freedman et al. 1994); however, due to the large predicted distance of NGC 4603 ( $>20$  Mpc), we could expect to find only the longest period Cepheids (i.e.,  $P \gtrsim 25$  days). In fact, if NGC 4603 were located at  $\gtrsim 45$  Mpc, Cepheids in this galaxy would be too faint to discover at all with the WFPC2 instrument. We thus tried to optimize our observing sequence to facilitate the discovery of longer-period variables. Our original plan was to perform 8 F555W visits over the course of  $\approx 60$  days in 1996, spaced to maximize our ability to detect and parameterize Cepheids with a variety of periods (as described in Freedman et al. 1994). Unfortunately, the final observation planned for 1996 did not occur due to an HST safing event. Our sensitivity for the longest-period Cepheids — exactly those which are brightest and easiest to find — is therefore limited; those detected suffer from substantial aliasing in period determination. Details of the observations performed are listed in Table 1. In Figure 1, we show the results of a simulation for the expected error in period determination as a function of period for the sampling ultimately used, illustrating the effects of aliasing.

## 3. DATA ANALYSIS

### 3.1. Photometry

The data were calibrated via the standard Space Telescope Science Institute pipeline processing (Holtzman et al. 1995), applying the Hill et al. (1998) long-exposure magnitude zero point. Each frame was also corrected for vignetting and geometrical effects on the effective pixel area as described in Stetson et al. (1998).

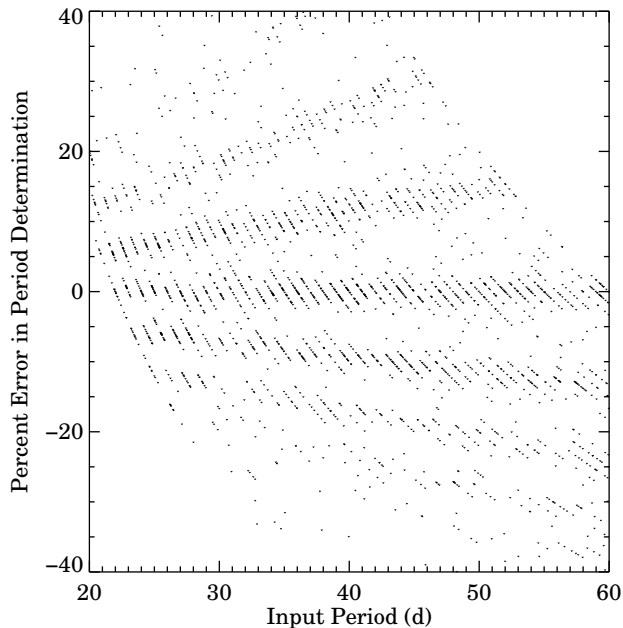


FIG. 1.— The percentage difference between the period measured using our algorithms and the actual period for simulated observations of stars with Cepheid light curves of a variety of phases and amplitudes measured (with realistic magnitude errors appropriate for stars with  $F555W=27.3-27.5$ ) at the epochs of our actual observations, as a function of period. The period errors are dominated by mistakenly identifying an alias as the actual period. The diagonal striping apparent here is due to the gridding in period used for fitting template light curves.

Background levels in the data frames were high enough and exposure times long enough that neither charge transfer inefficiencies nor variations in the photometric zero points with exposure time should significantly affect our results (cf. Rawson et al. 1997 and references therein). Each of the WFPC2 chips was analyzed separately. Because the second WF chip contained the nucleus of NGC 4603, crowding was severe and few stars could be resolved in it; that chip was therefore omitted from analysis. The fourth WF chip was directed at an outer portion of the galaxy, containing few stars and no significant numbers of Cepheids; it, too, was therefore removed from our analysis.

Photometry was then performed on each of the data frames using the DAOPHOT II/ ALLFRAME package (Stetson 1987). As an independent check, magnitudes were also obtained using a version of DoPHOT (Schechter, Mateo & Saha 1993) modified by Abi Saha for use with HST data (see, e.g., Ferrarese et al. 1996). The DoPHOT reductions were used as a consistency check only; the analysis presented in this paper is based on the ALLFRAME photometry alone. For F555W observations, the two sets of photometry agreed to within  $\pm 0.08$  magnitudes on average; this agreement is consistent with that found for distant galaxies observed as part of the Key Project (e.g., Ferrarese et al. 1996, Silberman et al. 1998). The ALLFRAME analysis was more extensive and resulted in larger

numbers of Cepheid candidates; for candidates found using both packages, the agreement in period was found to be well within the errors quoted below.

For the ALLFRAME photometry, procedures similar to those of the HST Key Project on the Extragalactic Distance scale were used (see, e.g., Kelson et al. 1996 for a more detailed description). ALLFRAME performs photometry by fitting a predefined point-spread function (PSF) to all stars on a frame and iteratively determining their magnitudes. Files describing the WFPC2 PSF and its variation across the field (determined from observations of globular clusters; cf. Hill et al. 1998) were provided by P. Stetson. For each epoch, up to six HST frames were obtained, and thus up to six measurements of each star’s magnitude were made. Those measurements are sometimes contaminated by cosmic rays or other transient phenomena. Although ALLFRAME attempts to limit their effect, it was found that simply averaging the magnitudes determined using ALLFRAME and weighting them according to their error estimates sometimes yields very inaccurate results. We therefore experimented with a number of robust estimators for the mean of the ALLFRAME measurements (including median, Tukey bi-weight, and trimean; cf. Beers et al. 1990) using the magnitudes of artificial stars inserted (using the ALLFRAME PSF) on our data frames. The most successful proved to be an iterative reweighting method described by Stetson (1997). In this technique, each measurement’s weight is altered according to its difference from the prior estimate of the mean (taken to be the median of the epoch’s measurements for an initial guess), as implemented here according to the formula:

$$\sigma_i'^2 = \frac{\sigma_i^2}{1 + \left(\frac{m_i - \bar{m}}{2\sigma_i}\right)^2}, \quad (1)$$

where  $m_i$  is the  $i$ th measurement,  $\sigma_i$  is the error estimate in that quantity after the prior iteration, and  $\bar{m}$  is the estimate of the mean from the prior iteration; after this adjustment of the weights, a new determination of the mean is made.

An estimate of the uncertainty in each epoch’s mean magnitude measurement was obtained from the weighted standard deviation of the data:

$$\sigma_m^2 = \frac{\sum \frac{(m_i - \bar{m})^2}{\sigma_i^2}}{\sum \frac{1}{\sigma_i^2} (n - 1)}, \quad (2)$$

where  $n$  is the total number of measurements used in determining  $\bar{m}$ . The resulting uncertainty estimates were generally accurate to 10-20 % (based upon the median  $\chi^2$  of the comparison of each epoch’s magnitude measurements for a star to the mean magnitude obtained from all F555W measurements for that star).

An additional potential source of photometric errors is the estimation of the background counts underlying the star (due to unresolved stars, H II regions, etc.). ALLFRAME estimates that background level by taking the median number of counts from pixels within some annulus about the star whose magnitude is being measured. Initially, our studies were done using an annulus from 3 to 20 pixels in radius from the stars; we later performed photometry using background annuli from 3 to 10 pixels and from

3 to 6 pixels. For  $F555W$  observations of faint stars with well-determined photometry, the mean change in epochal magnitudes was  $0.000 \pm 0.001$  mag, the RMS 0.10 mag, and the root median square difference (also known as the probable error) 0.047 mag when photometry was done with a 3-10 pixel radius sky annulus instead of 3-6. For  $F814W$ , the corresponding numbers were  $0.000 \pm 0.003$  mag, 0.18 mag, and 0.079 mag. Somewhat larger differences resulted from changing from a 3-10 pixel background annulus to 3-20, though increasing the background region does reduce the scatter among the magnitude measurements for a given star. Therefore, for the mean magnitudes presented here, we have adopted the 3-10 pixel background level and included the probable magnitude error within the uncertainty estimate for each star's magnitude.

We found that using the ALLFRAME error estimates for weighting when averaging magnitudes for a given star yielded a systematic bias towards the brighter measurements. This bias is minimal when errors are small, but is several tenths of a magnitude for the faintest stars. We have chosen to perform averaging of magnitudes rather than fluxes as it yielded a lower scatter of epochally averaged magnitudes in tests of both artificial and actual stars, and our ability to discriminate variations in brightness from the effects of magnitude measurement errors was a major limiting factor in this work; a much smaller but significant bias in the opposite sense was also found for flux averaging. A comparison of the averaged  $F555W$  magnitudes for stars on Chip 1 to their unbiased median magnitude measurements may be found in Figure 2, along with a functional fit to the bias (here and in the remainder of the paper,  $F555W$  and  $F814W$  will refer to magnitudes obtained by combining ALLFRAME measurements with an appropriate zero point; no aperture or bias corrections have been applied to them.  $V$  and  $I$  will be used to refer to fully corrected magnitudes on the Johnson and Kron-Cousins systems, respectively). Such functional fits were used in a Brent's method-based algorithm (cf. Press et al. 1992) to remove the biases in mean  $V$  and  $I$  magnitudes before color measurements or comparison to Cepheid P-L relations. Any biases due to averaging procedures should be corrected via this method. The expected error in the amount of the bias correction due to errors in measuring a star's mean magnitude is much less than the width of the P-L relation in both  $V$  and  $I$  ( $\sim 0.04$  mag for typical candidate Cepheids in our dataset), and thus should have no effect on our final results.

### 3.2. Cepheid Identification

NGC 4603 is the most distant galaxy for which a Cepheid search has been attempted; the required photometry presented a considerable challenge. Because the errors in the magnitude measurements for each epoch were a substantial fraction of typical Cepheid amplitudes and because of the limited number of epochs available, common techniques for identifying variables (see, e.g., Rawson et al. 1997 and references therein) proved to be of limited utility; for instance, the phase dispersion minimization method, which requires binning the observations in phase, is hardly optimal for noisy datasets with such a limited number of observations (Stellingwerf 1978). We instead have adopted an alternative approach loosely based on that described in Stetson 1996.

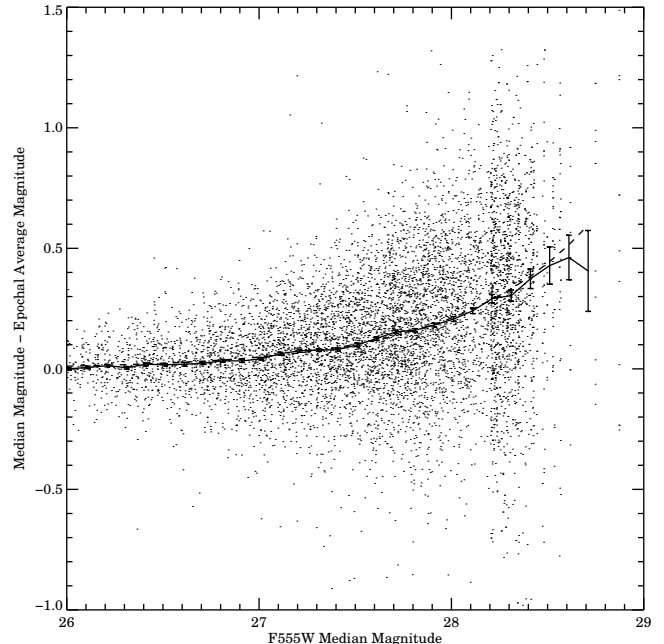


FIG. 2.— A plot of the difference between the unbiased median magnitude measurement for a star and the biased epochal average measurements. It is readily apparent that this bias is greater at fainter magnitudes. The solid line traces the median bias for stars in 0.1 mag wide bins, with error bars corresponding to the standard error of the mean for each bin; the dashed line is a regression fit to that data, showing that the bias is well represented by a power law in the actual (as opposed to measured) flux. So long as there exists a one-to-one correspondence between the unbiased actual and biased measured magnitudes (which is true for measured  $F555W < 28.125$ ,  $F814W < 27.166$ ), we may use this fit relation to correct for the bias.

The computing power of modern workstations is now sufficient that we could attempt to fit the photometry for every well-observed star to a grid of model Cepheid light curves (taken from Stetson 1996) with a wide range of periods and phases (in general, we sampled the period in 1 day increments and phase in increments of 0.025 for our variable search). This reduces the problem to a set of linear regressions to obtain mean magnitude and amplitude, a quite rapid procedure. By minimizing  $\chi^2$  on this grid, we obtain an estimate of the most appropriate Cepheid light-curve parameters for a given star. Nonvariable stars emerge from this fitting process with low amplitudes, typically substantially smaller than the amplitude error estimates resulting from the procedure; they can be rejected on this basis. For variables, the width of the minimum in the variation of  $\chi^2$  with period allows us to estimate our uncertainty in that parameter for a given star. We also confirmed our light-curve fits by performing a nonlinear  $\chi^2$ -minimization fit to the data for suspected variables with our best-fitting parameters as initial guesses. This generally resulted in minimal changes in parameters, indicating that our grid was sufficiently fine.

There are complications for longer-period variables ( $> 40$ d), for which multiple deep minima in  $\chi^2$  appear due to aliasing. However, our Monte Carlo analysis (see

§3.3.2) indicates that we still determine the periods of such Cepheids to 10-20 % accuracy (with the period errors then dominated by the spacing between the minima, reflecting the possibility that the deepest  $\chi^2$  minimum occurs at an alias — typically the nearest one — of the actual period, as reflected in Figure 1).

Stetson (1996) also defines model Cepheid  $I$ -band light curves based upon the same parameters as those for  $V$ . Thus, once a  $V$ -band fit is obtained, two determinations of the mean  $I$  magnitude for a star can be made by combining our two epochs' magnitude measurements and the expected  $I$  variation at the phase of those measurements (a method not unlike that described in Sandage et al. 1997). We used a weighted mean of these two determinations to estimate the mean  $I$  magnitude for our variables.

### 3.3. Simulations of Cepheid Detection Rates and Expected Errors

Because the Cepheids we are looking for are so faint, it is critical to confirm our ability to unambiguously detect such stars and to limit contamination of our sample of Cepheids with nonvariable stars. We therefore performed our variable search on two sets of artificial photometric data, one consisting of intrinsically nonvariable stars and one of stars changing in brightness (before measurement errors) according to template Cepheid light curves. For each star in one of these datasets, artificial magnitude measurements were made according to the actual timing of the HST visits. To account for the possibility of non-Gaussian distributions of errors, these constant or varying light curves were modified by numbers selected randomly from the set of actual deviations of  $F555W$  or  $F814W$  magnitude measurements of stars in a given magnitude range from their overall robustly determined mean magnitude (which, having been found from 48 or 12 magnitude measurements, respectively, were much more accurate than a single-frame measurement). To retain the information on a measurement's quality present in the ALL-FRAME error estimates, each frame's magnitude measurement in the artificial datasets was assigned the magnitude uncertainty estimate from the appropriate star and frame number for the measurement error applied. This analysis was performed for stars in ten 0.2 magnitude wide ranges, equivalent to  $F555W$  magnitudes from 26.3-26.5 to 27.7-27.9.

#### 3.3.1. False Positives

Attempting to find variables in our fake photometry of nonvariable stars generates candidate “variables” that mimic real Cepheids, hereafter referred to as “false positives.” The rate of these misidentifications in the NGC 4603 dataset is such that any reasonable list of candidate Cepheids we may produce will be contaminated with nonvariable stars. However, using our simulations, we have been able to find a number of criteria that can help reject such candidates. Some results of these simulations are plotted in Figures 3-5.

Foremost, the majority of the false positives possess low amplitudes ( $<0.6$  magnitudes peak-to-peak in the principal Fourier component, the form of amplitude measured by our template fitting technique), as illustrated by Figure 4, so excluding low-amplitude variables eliminates many

of them. We also exclude stars with low amplitudes compared to their statistical error estimates from least-squares fitting. A further test that proved very useful was to require all candidate Cepheids to have at least four data points more than  $1.2\sigma$  away from their robustly determined overall mean magnitude; nonvariable stars rarely possessed that many deviating points. This is effectively a test for a non-Gaussian distribution of magnitude measurements (a characteristic of Cepheid light curves) that is resistant to a small number of outliers. Another helpful restriction was ruling out very short period ( $< 24$ d) candidates, as those were far more likely to be false positives than real Cepheids (due to the increasing ability to make a given light curve match given magnitude variations with some choice of phase at shorter periods). All results discussed in this paper utilize variable-finding routines that perform all of these tests. The number of nonvariable stars which survive our variability criteria is fairly low; as shown in Figure 3, on Chip 1 (the Planetary Camera, which has the deepest effective photometry) we find that  $\sim 0.5\%$  of all faint stars with  $F555W \simeq 27$  (but up to  $6\%$  by  $F555W = 27.6$ ) may be misclassified as Cepheids in our analysis.

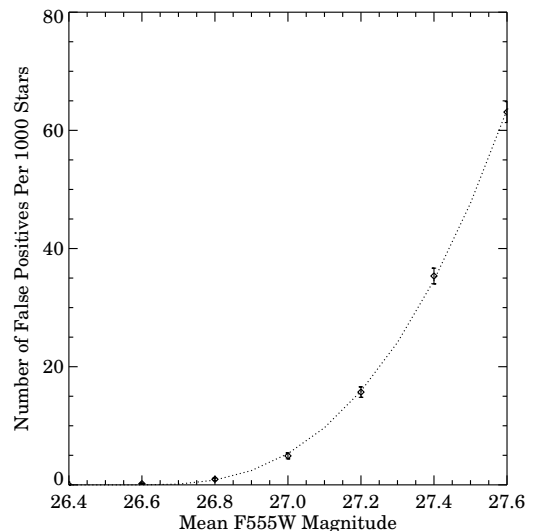


FIG. 3.— Results of simulations for the rate at which false positives occur for stars on Chip 1 (the Planetary Camera) as a function of  $F555W$  magnitude using our variability criteria, which have excluded the great majority of such misidentified stars. In this and all following figures, the dotted line indicates the fit used in obtaining maximum likelihood estimates of distance (see §3.1).

Given the large numbers of faint stars in our dataset, it is likely that our list of candidate Cepheids contains many which are actually nonvariable. There were roughly 3000 stars with well-determined photometry (i.e., magnitude measurements on  $> 90\%$  of all frames) on Chip 3, which has the most stars found; there are roughly 2100 such stars on Chip 1 (the Planetary Camera). We searched for Cepheids among these. Integrating the false positive rate over our observed magnitude distributions, we expect  $34.0 \pm 5.8$  on Chip 1, and  $56.9 \pm 7.5$  on Chip 3. In contrast, 61 stars on Chip 1 (all of  $F555W$  magnitude 27 or

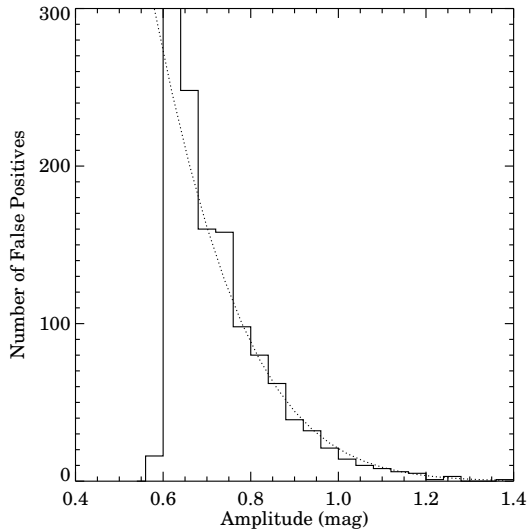


FIG. 4.— Results of simulations for the distribution of false positives in amplitude for magnitudes typical of our Cepheid candidates. Stars with measured amplitude below 0.60 mag were rejected as Cepheid candidates.

fainter) and 69 on Chip 3 passed all our Cepheid detection tests. Therefore, we concluded that the set of putative variables on Chip 3 is too contaminated to yield useful information, and we have concentrated on the candidate Cepheids on Chip 1 for further analysis.

### 3.3.2. Artificial Cepheids

To determine our ability to detect any variable stars present in our dataset, we generated data with realistic photometric errors determined as described above applied to analytically defined Cepheid light curves (Stetson 1996) with randomly selected periods, amplitudes, and phases. These “artificial Cepheid” Monte Carlo simulations yielded encouraging results. On both the Wide Field and Planetary Camera chips, 45-70 % (depending upon input parameters; the recovery rate was substantially less than this for candidates with input amplitudes below 0.6 mag, as should be expected given our variability criteria) of those Cepheids with mean  $F555W \lesssim 27.5$  passed our tests, with probable magnitude measurement errors of  $\lesssim 0.1$  mag and period errors of  $\sim 10\%$ , quite comparable to the uncertainty estimates from our variable search routines. Some of the results of these simulations are presented in Figures 6-9.

## 4. RESULTS

A number of potential Cepheid variables on Chip 1 with well-determined parameters were found. Light curves for some of these candidates are shown in Figure 10. Their properties are summarized in Table 2. Epochal photometry and light curves for all candidate Cepheids are available via WWW.<sup>7</sup>

<sup>7</sup><http://www.astro.berkeley.edu/~marc/n4603/>

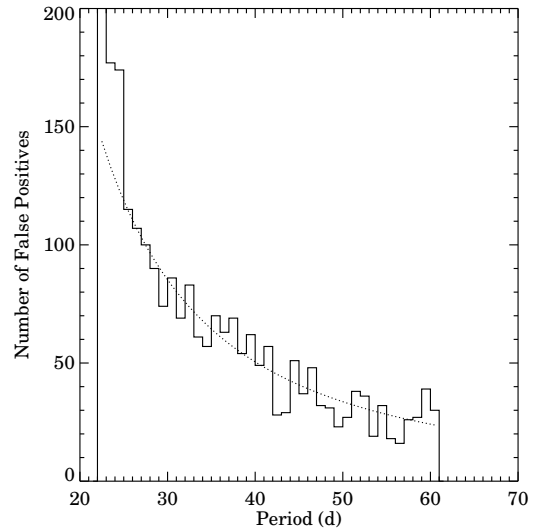


FIG. 5.— Results of simulations for the distribution of false positives in period, for magnitudes typical of our Cepheid candidates. Stars with measured period less than 24 d or greater than 60 d were rejected as Cepheid candidates.

The  $F555W$  and  $F814W$  mean magnitudes of the variables determined from the chi-squared minimization were converted to Johnson  $V$  and Kron-Cousins  $I$  using equations from Hill et al. (1998):

$$V = F555W - 25 - 0.052(V - I) + 0.027(V - I)^2 + 22.510 \quad (3)$$

$$I = F814W - 25 - 0.063(V - I) + 0.025(V - I)^2 + 21.616, \quad (4)$$

where  $F555W$  and  $F814W$  are the measured ALLFRAME magnitudes for the corresponding filters. Fixed aperture corrections of  $-0.17 \pm 0.01$  magnitudes each, determined based on those obtained in prior Key Project ALLFRAME analyses for the PC (Graham et al. 1998), were also applied when obtaining the  $V$  and  $I$  magnitudes.

### 4.1. Maximum Likelihood Analysis

In order to extract as much of the information available from our set of candidate Cepheids as we can despite the presence of false positives, we have performed an extensive maximum likelihood analysis to determine the distance modulus of NGC 4603. This required knowledge of our variable detection rates and the errors in measuring the period and magnitude of actual Cepheids, in addition to the distribution in period, magnitude, and amplitude of false positives; these could all be obtained from our Monte Carlo simulations (q.v. above). To perform the maximum likelihood analysis, we also required some knowledge of the distribution in period of actual Cepheids; this was

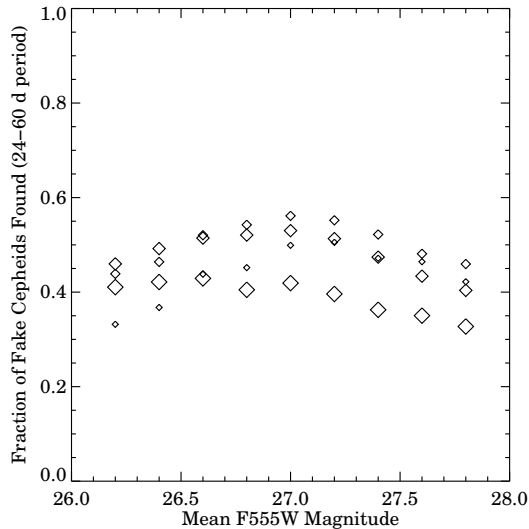


FIG. 6.— Results of simulations for the rate at which our algorithms detect Cepheid variables of a given  $F555W$  magnitude. The data are divided into subgroups according to the periods of the simulated Cepheids (with the largest symbols used for the average detection rate for those stars with the longest periods of variation, and the smallest the shortest). The dependences of the variable detection rate upon period and amplitude were complex and nonseparable, requiring us to interpolate upon a grid of simulation results in our maximum likelihood analysis.

found through a power-law fit to the long-period tail of the distribution of Large Magellanic Cloud (LMC) Cepheids in Alcock et al. 1999 to be roughly proportional to the  $-2.0$  power of period (defining the parameter  $\alpha$  used below; i.e., we have adopted a differential distribution of Cepheids in period of the form  $N(P_R)dP_R \propto P_R^\alpha dP_R$ ). Even violently changing this assumption (changing  $\alpha$  by  $\pm 1$ ) led to changes in the derived distance modulus of less than  $0.10$  mag. For the purpose of this analysis, we adopt the LMC Cepheid Period-Luminosity relations of Madore & Freedman (1991) (and, for the likelihood analysis, the dispersions of LMC Cepheids about that relation) which have been used by the Key Project on the Extragalactic Distance Scale.

There are two distribution functions required for this analysis, labelled hereafter as  $f_{real}$  and  $f_{false}$ . These represent the probability that a particular star is a real Cepheid and detected with given properties, or a nonvariable star and identified as a Cepheid with those properties, respectively. Based upon the results of our simulations, the former is defined as a function of observed period  $P$ , magnitude  $m$ , and amplitude  $A$ , and of the given distance modulus  $m - M$  as

$$f_{real}(m, P, A|m - M) \sim p_{detect}(m, P, A) \frac{1}{2\pi\sigma_m\sigma_P} \quad (5)$$

$$\times \int_{P_{min}}^{P_{max}} e^{-\frac{(P-P_r)^2}{2\sigma_P^2}} e^{-\frac{(m-m_r)^2}{2\sigma_m^2}} P_r^\alpha dP_r,$$

where  $p_{detect}(m, P, A)$  is the probability of our detecting a Cepheid that has a given observed magnitude, period, and amplitude,  $P_r$  is the actual, as opposed to

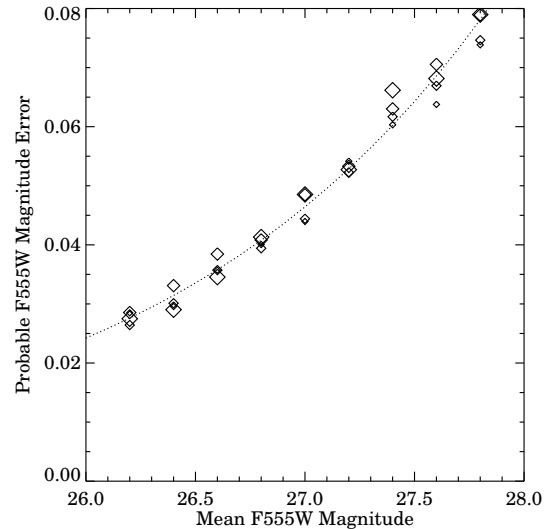


FIG. 7.— Results of simulations for the probable error in measuring the mean  $F555W$  magnitude of a Cepheid as a function of  $F555W$  magnitude. No trend in this quantity is seen either with the period or amplitude of the Cepheid's variation; in this plot, as in Figure 6, symbols of larger size represent errors for longer-period variables. In our maximum likelihood analyses, probable errors are multiplied by an appropriate correction factor, 1.48260, to yield the corresponding Gaussian  $\sigma$ .

observed, period of a Cepheid,  $m_r$  is the ideal magnitude of a Cepheid for a given distance modulus and  $P_r$  (from the Madore & Freedman P-L relation), and  $\alpha$  is treated as a constant parameter for the maximum likelihood analysis describing the distribution in period of actual Cepheids. In our Monte Carlo analysis,  $\sigma_P$  proved to be a complex function of period, amplitude, and magnitude, while  $\sigma_m$  was significantly dependent only on magnitude (as applied in the maximum likelihood analysis,  $\sigma_m$  has added to it in quadrature contributions from the dispersion of the P-L relation and estimates of magnitude measurement errors due to background subtraction and bias correction uncertainties). Because of their complicated dependence on all possible variables, values of  $v$  and  $\sigma_P$  were obtained by interpolating within a  $9 \times 9 \times 9$  grid in period, amplitude, and magnitude containing the results of simulations for these quantities. The values of  $\sigma_m$  were taken from least-squares fits of empirically chosen functions to the Monte Carlo results. Once a distance modulus is chosen,  $f_{real}$  is normalized to make the expectation value of the number of Cepheids existing in our dataset unity:

$$\sum_i n_i \int f_{real}(m_i, P|m - M) dP = 1, \quad (6)$$

where  $m_i$  is the mean magnitude in a bin ( $0.04$  mag wide in our analysis) and  $n_i$  is the number of observed stars with good photometry in that bin. The actual number

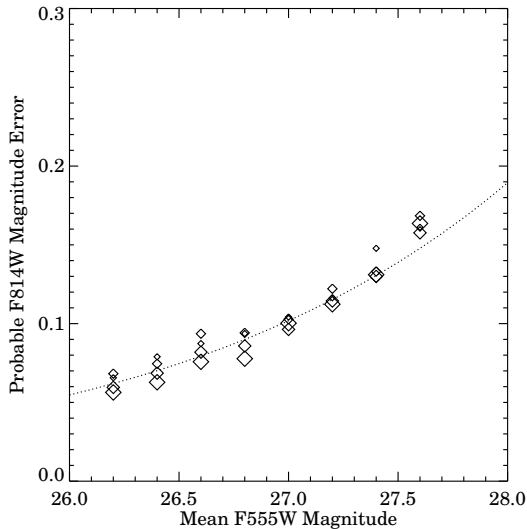


FIG. 8.— Results of simulations for the probable error in measuring the mean  $F814W$  magnitude of a Cepheid as a function of  $F555W$  magnitude. No trend in this quantity is seen with the period or amplitude of the Cepheid’s variation.

of Cepheids in the data will then be a parameter whose value is determined by the likelihood analysis. This integral is performed numerically in 1 day increments over the range of periods accepted for candidates, 24-60 days. This normalization may not be perfect, particularly for the  $I$  analysis, so much more significance should be ascribed to, e.g., results for the difference of the number of Cepheids from zero than to the exact number of Cepheids found.

The chance that a given unvarying star is selected as a candidate variable of given properties,  $f_{false}$ , was found via our simulations to be proportional to a power law in period and a Gaussian (of zero mean) in amplitude:

$$f_{false}(m, P, A) \sim \frac{1}{\sqrt{2\pi}\sigma_A} e^{-\frac{A^2}{2\sigma_A^2}} P^\beta; \quad (7)$$

in our Monte Carlo simulations,  $\sigma_A$  proved to be a function of the magnitude alone and  $\beta$  a constant. Because these parameters are independent of period and amplitude,  $f_{false}$  may be integrated over these variables analytically. This distribution was then normalized such that its integral over the possible periods and amplitudes for candidates was 1; for an individual candidate, it must be multiplied by the overall rate of false positives at a given magnitude,  $r(m)$ , to yield the probability that that star is a false positive.

The functional fits to the parameters required by the maximum likelihood analysis used were:

$$\begin{aligned} \sigma_{m_V}(m_V) &= 0.1 \times 10^{-0.2824(28.18-m_V)} \\ \sigma_{m_I}(m_V) &= 0.2 \times 10^{-0.2696(28.09-m_V)} \\ \sigma_A(m_V) &= \max(0.08, -2.013 + 0.0791m_V) \\ \beta &= -1.82 \\ r(m_V) &= \max(0.05350 \times (m_V - 26.6)^{2.714}, 0), \end{aligned} \quad (8)$$

where  $m_V$  is the  $F555W$  magnitude of a given star before aperture corrections and  $m_I$  its corresponding  $F814W$  magnitude.

The logarithm of the likelihood is then defined as

$$\begin{aligned} \ln \mathcal{L} &= \sum_{i=1}^{n_{cand}} \ln [N_{Ceph} f_{real}(m, P, A | m-M) + r(m) f_{false}(m, P, A)] \\ &+ \sum_{j=1}^{n_{bin}} n_j \ln [(1 - N_{Ceph} f_{real}(m_j | m-M)) (1 - r(m_j))], \end{aligned} \quad (9)$$

where  $n_{cand}$  is the total number of Cepheid candidates,  $n_{bin}$  is the number of magnitude bins used, and  $N_{Ceph}$  is roughly equivalent to (and directly proportional to) the number of observed Cepheids in the dataset, an unknown in the analysis. The first summation corresponds to the product (before the logarithm) of the probabilities that our candidate Cepheids will be detected as such stars with their given properties; the second, the product of the probabilities that each of our non-candidate stars are not either detected Cepheids or false positives. The logarithm of the likelihood, and thus the likelihood itself, is maximized over a grid in the distance modulus  $m - M$  and the number of Cepheids in the dataset  $N_{Ceph}$ . Note that for the non-candidates, the distribution functions have been integrated over period and amplitude.

We have tested our maximum likelihood techniques by applying them to datasets containing both nonvariable stars (potentially false positives) and a set of simulated Cepheids with a fixed distance modulus and a realistic distribution of properties. If the number of real Cepheids was large enough and NGC 4603 placed near enough that

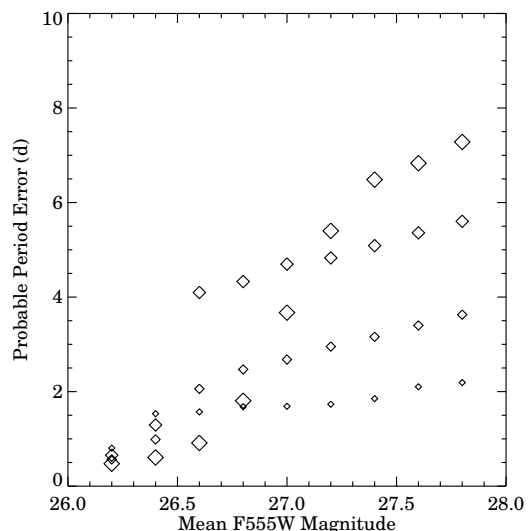


FIG. 9.— Results of simulations for the probable error in measuring the period of a Cepheid as a function of magnitude. Like the Cepheid detection rate, this quantity proved to be dependent on period and amplitude in a complex, nonseparable fashion; therefore, interpolations of the results of simulations were used for it in our maximum likelihood analysis. Due to aliasing, the longest-period Cepheids have the greatest errors in period determination (as can be seen in Figure 1).



a significant number of the input Cepheids are found by the variable search procedure, then our techniques effectively recovered the input distance. If those conditions are not met, the highest-likelihood solutions generally prove to be those in which the number of Cepheids in the dataset is minimized or the distance modulus is maximized, i.e., cases in which the chance of observing a Cepheid would be as small as possible. Such solutions are easy to recognize and did not occur in our analysis of NGC 4603.

This analysis was performed independently using the  $V$  and  $I$  mean magnitudes of our candidates to determine the distance modulus. From the  $V$  analysis, we determine that the hypothesis of no Cepheids present is excluded at  $> 9\sigma$ , that  $43 \pm 7$  actual Cepheids are present in our dataset, and that NGC 4603 has a distance modulus of  $33.15^{+0.11}_{-0.10}$  ( $1\sigma$  random errors) before correction for metallicity and dust extinction. The  $I$  analysis yields a poorer constraint, with a Cepheid signal present at  $> 7\sigma$  and an uncorrected distance modulus measurement of  $32.97^{+0.15}_{-0.09}$ . See Figures 11 and 12 for plots of the resulting likelihood contours. The location of our candidates in the NGC 4603 color-magnitude diagram is shown in Figure 13. Figures 14 and 15 illustrate the differences between the distributions of candidate Cepheids in magnitude and color and those expected for false positives. The excess candidates beyond the false positives do seem limited in their brightness and colors in the fashion expected for Cepheids of a variety of periods and reddenings.

Since we have obtained substantial knowledge about the distribution in properties of real Cepheids and false positives through our maximum likelihood analysis, we can estimate the probability that a given candidate is in fact a Cepheid; the resulting probabilities are listed in Table 2.  $V$  and  $I$  period-magnitude plots for the potential Cepheids we have found in NGC 4603 (containing essentially the

same information) may be found in Figures 16 and 17. Those candidates found to have greater than 50 % probability of being Cepheids in both the  $V$  and  $I$  maximum likelihood analyses have their simulation-based error bars (as used in the analyses) depicted on the plots.

Such higher-probability candidates may be used to provide an illustration of the workings of our maximum likelihood procedure. These stars should have a relatively high value of  $f_{real}$ , so they must agree with the expected magnitude of a Cepheid of the same measured period given our choice of distance modulus within the estimated errors. However, they should also have a relatively small value of  $r(m)f_{false}$ . Given the strong magnitude dependence, we expect such stars to be brighter than the typical candidate. Thus, if we were to calculate the mean distance modulus predicted from the properties of such stars, we would expect it to be fairly consistent with but biased low compared to that obtained from the full maximum likelihood analysis. This is borne out by such a calculation for, e.g., those stars that have  $> 80\%$  probability in both the  $V$  and  $I$  analyses; they give a value of  $32.95 \pm 0.10$  for the  $V$  modulus and  $32.80 \pm 0.08$  for  $I$ , 0.20 and 0.17 mag less than those obtained from the full procedure. The maximum likelihood technique does not simply determine a distance modulus weighting stars according to their probability of being Cepheids, but instead incorporates as much information as possible about how effectively we can find such stars, minimizing incompleteness/Malmquist-type biases.

#### 4.2. Uncertainties and Corrections

In addition to the statistical uncertainties in our measurements of the distance modulus of NGC 4603, which

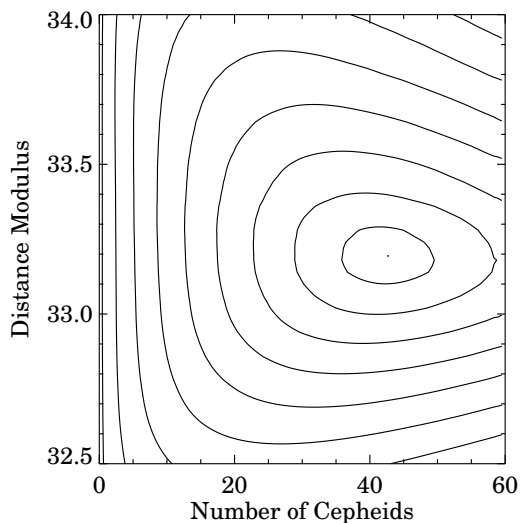


FIG. 11.— Results of our maximum-likelihood analysis using  $V$  mean magnitudes of candidate Cepheids to determine the distance to NGC 4603. The contours represent 1,2,3,4, etc.  $\sigma$  limits on the measured parameters. We confirm that Cepheids are present in our data set at  $> 9\sigma$ .

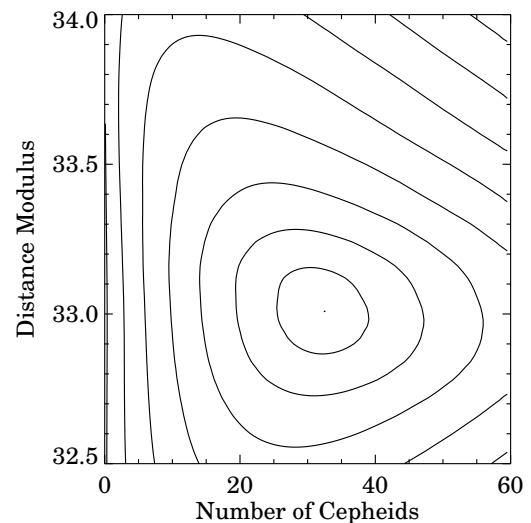


FIG. 12.— Results of our maximum-likelihood analysis using  $I$  mean magnitudes of candidate Cepheids to determine the distance to NGC 4603. The contours represent 1,2,3,4, etc.  $\sigma$  limits on the measured parameters. We confirm the detection of Cepheids in the  $I$  band at  $> 7\sigma$ .

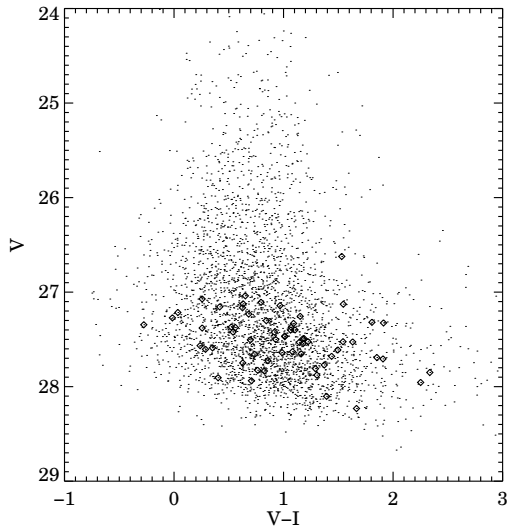


FIG. 13.— A color-magnitude diagram for stars on Chip 1. Candidate Cepheids are indicated by open symbols.

were determined by our maximum likelihood analysis, our results are also subject to a number of potential sources of systematic error. In this subsection, we will attempt to estimate the amounts of possible error due to the calibration of photometry and our analysis techniques, to uncertainties in the Cepheid P-L relation calibration, and to our limited knowledge of physical conditions in and towards NGC 4603, and make whatever well-established corrections possible to our distance moduli.

Uncertainties in the HST zero point of  $\pm 0.05$  magnitudes in  $V$  or  $I$  affect our measurements of the NGC 4603 distance in much the same fashion as Key Project distances (Hill et al. 1998), with one important difference: because the mean magnitudes of a given star are not as well determined, we are unable to use a measurement of  $E(V-I)$  to measure reddening, so relative zero point errors do not propagate into our results as they do in the Key Project methodology. A mean difference of 0.08 mag in  $V$  between DoPHOT and non-bias-corrected ALLFRAME photometry for our candidates was found. This may be due to differences in the characteristics of any biases that occur when averaging ALLFRAME and DoPHOT results at these faint magnitudes. We adopt the bias-corrected ALLFRAME results here and include half this difference as a potential systematic error in  $V$  magnitudes. In the absence of sufficient DoPHOT comparison photometry in  $I$ , we consider a 0.10 mag systematic error to be possible, though substantially larger than any found in prior studies.

We also must consider uncertainties in the distance modulus resulting from the maximum likelihood methodology and the Monte Carlo fits that were used to define  $f_{real}$  and  $f_{false}$ . Changing the assumed false positive rate radically (e.g., by 50%) altered the resulting distance modulus constraints by at most 0.09 mag in both  $V$  and  $I$ . Considering also the differences in measured distance modulus

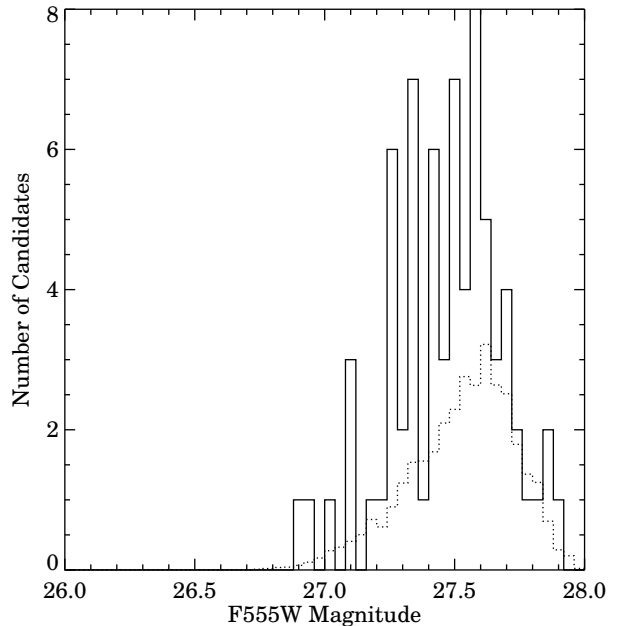


FIG. 14.— Histogram of the  $F555W$  magnitude distribution of candidate Cepheids (solid line) and that expected for false positives given the distribution in magnitude of observed stars (dashed line).

exhibited when the power-law parameter for the distribution in period of real Cepheids,  $\alpha$ , is changed by  $\pm 1$ , we find potential systematic errors in the maximum likelihood procedure of 0.14 mag for  $V$  and 0.12 mag for  $I$ . If we add the corresponding errors in quadrature, we find that systematic errors in photometry and in our analysis techniques should be less than 0.15 mag in  $V$  and 0.16 mag in  $I$ . Because we account for the lower probability of detecting faint Cepheids via our maximum likelihood technique and fix the slope of the P-L relation used, the effects of incompleteness bias should be minimal.

Our results are also subject to possible systematic errors in the calibration of the Cepheid P-L relation. Indeed, one of the largest remaining systematic uncertainties in the extragalactic distance scale is our limited knowledge of the distance to the Large Magellanic Cloud, which currently provides the fiducial standard Cepheid calibration. For the Key Project, this uncertainty has been taken to be  $\pm 0.13$  mag; we adopt this value so that if the distance to the LMC is better determined in the future our distance determination may be easily adjusted in concert with theirs. We also adopt the Key Project's estimate of potential errors within the LMC  $V$  and  $I$  P-L calibrations of  $\pm 0.05$  magnitudes (see, e.g. Rawson et al. 1997).

A number of potential systematic errors in our distance modulus could be the result of physical effects. First, as an Sc galaxy or, alternatively, one with maximum circular velocity of  $220 \text{ km s}^{-1}$  (Giovannelli et al. 1997), we may expect Cepheids in NGC 4603 to possess substantially higher

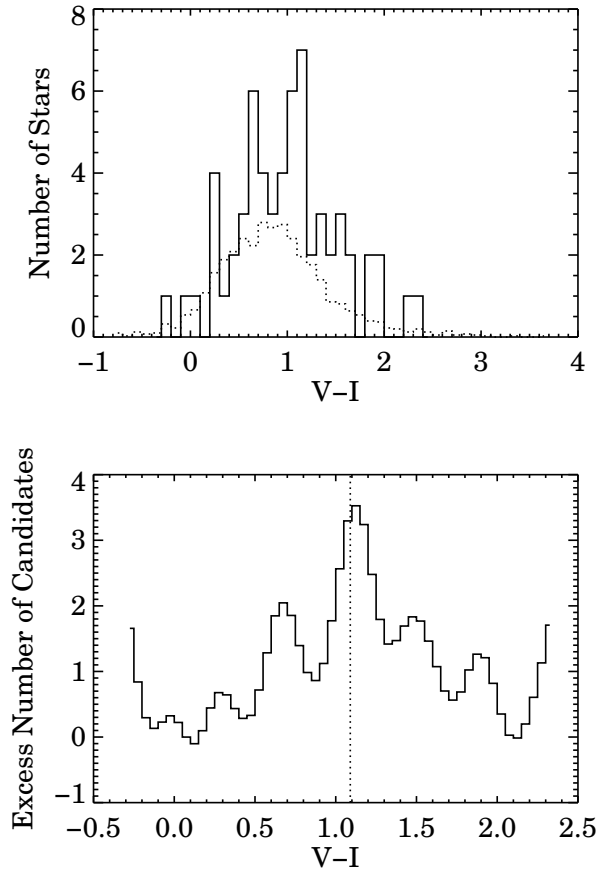


FIG. 15.— (upper panel) Histogram of the  $V - I$  colors of candidate Cepheids (solid line) and that expected for false positives given the color distribution of observed stars (dashed line). (lower panel) The difference between the two histograms, smoothed with a Gaussian kernel. The dotted line indicates the typical color expected for a Cepheid of period 35 d reddened by foreground Galactic dust as measured by Schlegel, Finkbeiner, & Davis (1998). The distribution appears very consistent with Cepheids of a range of reddenings, with no similar excess of blue stars.

metallicity than those in the LMC, by roughly  $0.40 \pm 0.20$  dex at the radius of the PC field (applying the results of Zaritsky, Kennicutt, and Huchra 1994 to obtain values for the typical metallicity and metallicity gradient in NGC 4603). Using the relation of Kennicutt et al. (1998), we should therefore expect that our distance modulus is an underestimate by  $0.096 \pm 0.081$  mag. It should be noted that other studies have found larger, but still statistically equivalent given the error bars, metallicity effects (Sasselov et al. 1997, Kochanek 1997, Nevalainen & Roos 1998), while theoretical calculations predict effects that are minimal or opposite in sign (Alibert et al. 1999, Musella 1999). We therefore make no correction, and consider the entire  $0.096$  mag to be a potential systematic error.

Another potential physical effect is extinction by dust along the line-of-sight to the Cepheids, either within NGC 4603 or our own Galaxy. Unfortunately, the Centaurus cluster lies behind a region where substantial emission from Galactic dust has been observed; the effect of

this dust should therefore be quite appreciable. We thus must correct the distance moduli we have found for Galactic foreground dust absorption of  $A_V = 0.54 \pm 0.08$  magnitudes ( $A_I = 0.33$  magnitudes, using a typical Galactic extinction law), taken from the extinction map of Schlegel, Finkbeiner & Davis (1998). After correction for foreground extinction, our data yield  $E(V - I)_{\text{internal}} = -0.04^{+0.14}_{-0.18}$  (random); we constrain the reddening due to dust within NGC 4603 only poorly. To place limits on its effects, we may safely assume that internal dust will yield  $E(V - I) \geq 0$ , of course; an examination of Key Project papers studying galaxies of similar inclinations indicates that  $E(V - I) < 0.07$  due to internal reddening is also a reasonable assumption. Conversion to  $A_V$  with a typical Galactic extinction law indicates that we might therefore expect that our  $V$  distance modulus should be reduced by as much as 0.17 mag in correcting for extinction by dust within NGC 4603, and our  $I$  modulus by as much as 0.10 mag. We thus adopt  $-0.09$  magnitude as an estimate of the possible  $1\sigma$  systematic error from internal extinction in  $V$ , and  $-0.05$  mag in  $I$ .

To estimate the total potential systematic errors, we add possible errors from physical effects in quadrature to the systematic uncertainties of the modulus from our photometric and maximum likelihood techniques and that from the P-L relation calibration, yielding total systematic

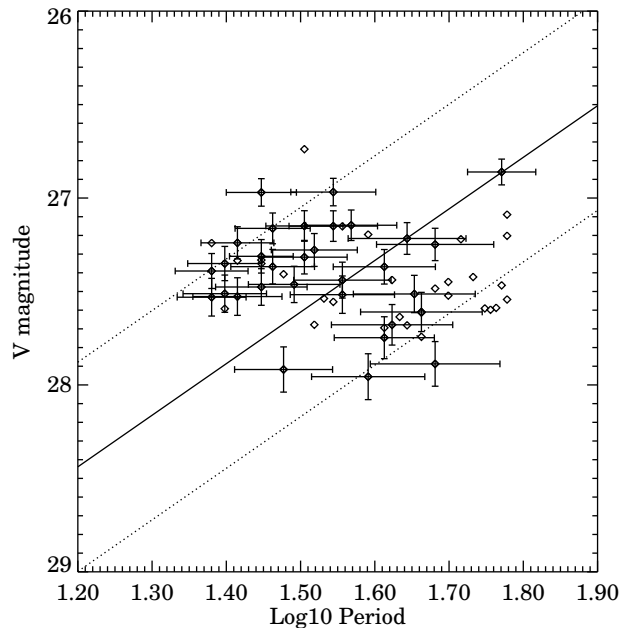


FIG. 16.— The  $V$  P-L relation for our candidate Cepheids. The solid line depicts the LMC P-L relation shifted to the distance modulus we have obtained; dotted lines indicate the  $2 - \sigma$  scatter of LMC Cepheids about that relation. Those candidates with more than 50% probability of being Cepheids in both the  $V$  and  $I$  analyses are plotted with the error bars used for them in the maximum likelihood analysis (drawn from our simulations).

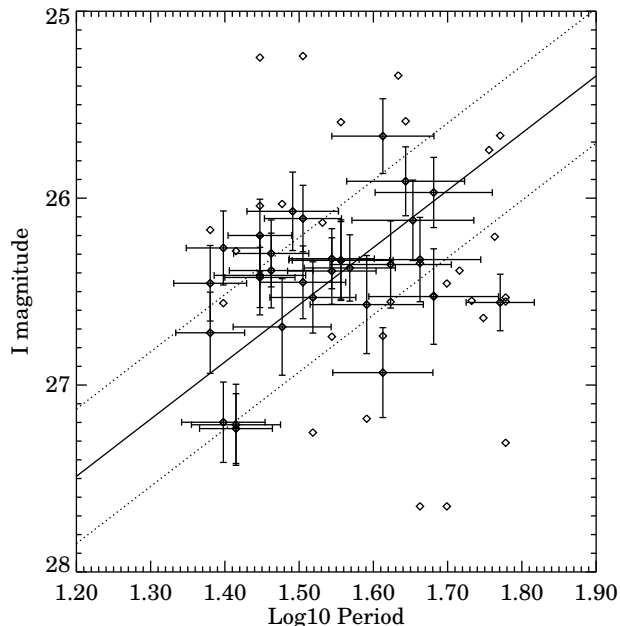


FIG. 17.— The  $I$ -P-L relation for our candidate Cepheids. The solid line depicts the LMC P-L relation shifted to the distance modulus we have obtained; dotted lines indicate the  $2 - \sigma$  scatter of LMC Cepheids about that relation. Those candidates with more than 50% probability of being Cepheids in both the  $V$  and  $I$  analyses are plotted with the error bars used for them in the maximum likelihood analysis (drawn from our simulations).

uncertainties of  $+0.23/-0.24$  magnitudes in  $V$  or  $\pm 0.23$  magnitudes in  $I$ . Combining all effects, we thus find from the  $V$  analysis that NGC 4603 has a distance modulus of  $32.61^{+0.11}_{-0.10}$  (random,  $1 \sigma$ )  $^{+0.24}_{-0.25}$  (systematic), corresponding to a distance of  $33.3^{+1.7}_{-1.5}$  (random,  $1 \sigma$ )  $^{+3.8}_{-3.7}$  (systematic) Mpc. The  $I$  analysis provides a quite consistent result, yielding a distance modulus of  $32.65^{+0.15}_{-0.09}$  (random,  $1 \sigma$ )  $\pm 0.24$  (systematic).

#### 4.3. Implications

Previous studies have obtained widely differing measurements of the distances to, and hence peculiar velocities of, Cen30 and Cen45, even when using the same techniques. Larger  $D_n - \sigma$  samples (e.g. that used in the Mark III catalog [Willick et al. 1997], which includes 22 galaxies in Cen30 and 9 in Cen45, as opposed to 9 and 4, respectively, in Faber et al.), for instance, have placed Cen30 as far as or even *behind* Cen45, with peculiar velocities of  $-110 \text{ km s}^{-1}$  and  $+1515 \text{ km s}^{-1}$  respectively, in great contrast to the earlier results. The hypothesis that Cen30 and Cen45 may lie at the same distance was first advanced by Lucey, Currie and Dickens (1986a) on the basis of a number of relative distance measures. It appears from some studies as though the Centaurus cluster may be in the midst of a substantial merger, with Cen45 falling into Cen30 and acquiring a rapid velocity thereby. On the other hand, some distance measurements, particularly those considered by Lynden-Bell et al. (1988), imply that Cen30 and Cen45 moving rapidly relative to the Local Group.

A flow of the center of mass of the Cen30/Cen45 system with such high speed – faster than the motion of the Local Group itself – would suggest the existence of a substantial attracting mass. From the results of the first  $D_n - \sigma$  studies, Lynden-Bell et al. (1988) hypothesized the existence of a “Great Attractor,” a large concentration of matter lying beyond the Centaurus cluster. However, neither optically nor *IRAS*-selected samples of galaxies have revealed regions of overdensity sufficient to explain these motions. In fact, according to redshift surveys, the Centaurus cluster itself, when combined with Hydra and Pavo-Indus-Telescopium on the other side of the galactic plane, should constitute the major local attractive point. Centaurus should therefore be approximately at rest in the Cosmic Microwave Background reference frame, and the bulk of the motion of the Local Group driven by its mass overdensity. In the Local Group frame one then expects to observe negative peculiar velocities in the direction of Centaurus, as there is expected to be a strong reflex dipole pattern from the motion of the Local Group itself. One possible explanation for the discrepancy between predicted and observed flows in this region has been provided by Guzman and Lucey (1993), who have suggested that  $D_n - \sigma$  distances can be compromised by age effects and that the large outflow of Centaurus is potentially suspect as a result; however, there is no particular reason to expect that galaxies in the Centaurus region should be younger than others in our neighborhood. If there is in fact only a very weak reflex signature in the velocity of the Centaurus cluster, the density parameter of the Universe must be very low, too low to explain the infall pattern around the Virgo supercluster.

The Cepheid distance measurement we have obtained may be used to set limits on such a flow. Our result is most easily compared to studies using other distance indicators and a peculiar velocity determination is most straightforwardly made by converting to velocity distance. This may be accomplished by multiplying the distance obtained by an appropriate value for Hubble’s Constant based upon the same calibration; we use the Key Project’s most recent estimate for Hubble’s Constant based upon Cepheid data analyzed similarly to that presented here,  $72 \pm 5$  (random)  $\pm 12$  (systematic)  $\text{km s}^{-1} \text{ Mpc}^{-1}$  (Madore et al. 1999). We then determine a velocity distance for NGC 4603 of  $2395 \pm 306$  (random)  $\pm 281$  (systematic)  $\text{km s}^{-1}$ . Note that this value should not be altered by any recalibrations of the zero point of the Cepheid distance scale because our distance measurements and those of the Key Project would be affected in the same way.

A variety of other estimates of the velocity distance of NGC 4603 and of Cen30 as a whole are presented in Table 3. To allow more effective comparison, the presumed velocity of Cen30 in the Local Group frame (“ $CZ_{Cen30, LG}$ ”) and number of galaxies included in each study are also listed; each of the  $D_n - \sigma$  samples in the table includes the preceding work as a subset.

Our result agrees well with estimates of the distance to Cen30 based on global analyses of the properties of cluster galaxies. Jerjen & Tammann (1997), for instance, find from an analysis of galaxy luminosity functions that Cen30 is  $1.63 \pm 0.15$  mag beyond Virgo. Taking the Virgo distance modulus to be  $31.07 \pm 0.07$  (random; from Freed-

man et al. 1998, excluding the  $3.9\sigma$  outlier NGC 4639 from the average), this yields distance modulus  $32.70 \pm 0.16$  (random). Studies of surface brightness fluctuations, too, find distances consistent with that we have obtained for NGC 4603; recent results of Tonry et al. (1999) yield a mean distance of  $2524 \pm 435$  (random) for 8 galaxies in Cen30.

Our result may also be compared to peculiar velocity predictions based on the gravity field inferred from the full sky *IRAS* survey or from surveys of optically selected galaxies (Nusser and Davis 1995). For example, using the gravity field derived for the *IRAS* 1.2 Jy survey and assuming  $\beta = 0.5$  leads to a predicted peculiar velocity  $v_p$  (in the LG frame) of  $14 \text{ km s}^{-1}$  versus a Cepheid inferred  $v_p$  of  $-74 \pm 306$  (random)  $\text{km s}^{-1}$  if the redshift of NGC 4603 is left at its observed value,  $cz_{lg} = 2321 \text{ km s}^{-1}$ , which should be appropriate if it is in fact a field galaxy. If we instead compare to the central redshift of Cen30,  $\approx 2807 \text{ km s}^{-1}$  in the Local Group frame (Lucey et al. 1986a), then its predicted  $v_p$  is  $-90 \text{ km s}^{-1}$ , while the Cepheid distance would imply  $v_p = 412 \text{ km s}^{-1}$ . The predicted and observed peculiar velocities disagree in this case by  $\sim 1.2\sigma$ .

Since we only have been able to perform a Cepheid distance analysis for one galaxy, we cannot claim to have established unambiguously the distance to the Centaurus cluster; while some studies have included NGC 4603 in Cen30, for instance, others have not. Indeed, as illustrated in Table 3, the location of Cen30 itself in redshift space, not only real space, has varied substantially from analysis to analysis, reflecting in no small part the large velocity dispersion and limited numbers of cluster spirals (Stein et al. 1997). It is worthy of consideration, though, that those studies that do exclude this galaxy from Cen30 place it nearer to us than the cluster itself (as in Willick et al. 1997, though the groupings used for Mark III spirals tend to place Cen30 at a substantially higher velocity than that found in other studies), lending support to the higher distance estimates for the cluster. At worst, our distance measurement should provide a lower limit on the distance to Cen30, and hence an upper limit on its peculiar velocity.

Our results are most easily reconciled with those of recent velocity-distance calibrated studies if NGC 4603 is treated as an object in the foreground of the Centaurus cluster. That is a rather reasonable scenario; previous studies (Bernstein et al. 1994, Willick et al. 1995, Willick 1999) have found that the Tully-Fisher distances of what are nominally cluster spirals correlate well with

their (rather than their clusters') redshifts. As a galaxy with a Tully-Fisher distance, NGC 4603 should be subject to the same selection effects. We note that the velocity distances determined from the two largest samples of Cen30 galaxies listed in Table 3 are in excellent agreement with each other though those distances were obtained via different methods and calibrated separately, and those measurements agree well with the *IRAS* 1.2 Jy survey-predicted peculiar velocity for Cen30. Our distance measurement for NGC 4603 is in good accord with a variety of Tully-Fisher measurements of the distance for that galaxy but agrees more poorly with the best measurements of the distance to Cen30 as a whole. Under very reasonable assumptions, we may conclude that Tully-Fisher distances, and therefore (based on their consistency for Cen30) those obtained via the  $D_n - \sigma$  technique as well, agree with the Cepheid distance scale and *IRAS*-predicted peculiar velocities to at least as far away as the Centaurus cluster.

The rough agreement of the results of this analysis with other studies of the Centaurus cluster is encouraging. For a firmly established Cepheid distance to Centaurus, a similar study would have to be performed on more galaxies, preferably including ones that show more definitive evidence of location in the cluster core (e.g. stripping of galactic gas) ensuring that members of Cen30 are observed. However, the substantial resources in HST time required with current instrumentation and the extremely extensive data analysis effort needed to produce a convincing result means that such efforts should most likely await the installation of the Advanced Camera for Surveys. Finding Cepheids at the distance of the Centaurus cluster is currently possible, but difficult indeed.

### Acknowledgements

We would like to thank Jay Anderson for his efforts to provide secondary photometry for this study and Jeff Willick for his assistance in interpreting Mark III data. We also would like to thank our program coordinators at STsCI, Doug van Orsow and Christian Ready, for their assistance, and the anonymous referee for helpful comments. This work was supported by NASA grants GO-06439 and GO-07507 from the Space Telescope Science Institute (operated by AURA, Inc. under NASA contract NAS 5-26555). J. A. N. acknowledges the support of a National Science Foundation Fellowship and the Berkeley Fellowship.

### REFERENCES

- Aaronson, M., et al. 1989, ApJ, 338, 654  
 Alcock, C. et al. 1999, AJ, in press, astro-ph/9811240  
 Alibert, Y., Baraffe, I., Hauschildt, P., & Allard, F. 1999, A&A, in press, astro-ph/9901294  
 Baker, J. E., Davis, M., Strauss, M. A., Lahav, O., & Santiago, B. X., 1998, ApJ, 508, 6  
 Beers, T. C., Flynn, K., & Gebhardt, J. 1990, AJ, 100, 32  
 Bernstein, G.M., Guhathakurta, P., Raychaudhury, S., Giovanelli, R., Haynes, M.P., Herter, T., & Vogt, N. P. 1994, AJ, 107, 1962  
 Branchini, E., et al. 1998, to appear in *Proceedings of the MPA/ESO Conference on Evolution of Large-Scale Structure: from Recombination to Garching*, eds. A.J. Banday, R.K. Sheth and L. Da Costa, astro-ph/9810106  
 Dekel, A. 1994, ARA&A, 32, 371  
 Dressler, A. 1993, in *Cosmic Velocity Fields*, ed. F. Bouchet & M. Lachieze-Rey (Gif-sur-Yvette: Editions Frontieres), 9  
 Faber, S.M., Wegner, G., Burstein, D., Davies, R.L., Dressler, A., Lynden-Bell, D., and Terlevich, R.J. 1989, ApJS, 69, 763  
 Ferrarese, L., et al. 1996, ApJ, 464, 568  
 Freedman, W. L., et al. 1994, ApJ, 427, 628  
 Freedman, W. L., Mould, J. R., Kennicutt, R. C. Jr., & Madore, B. F. 1998, astro-ph/9801080, preprint  
 Freudling & da Costa 1994, in *Cosmic Velocity Fields*, ed. F. Bouchet & M. Lachieze-Rey (Gif-sur-Yvette: Editions Frontieres), 187  
 Giovanelli, R., Haynes, M.P., Salzer, J.J., Wegner, G., Da Costa, L.N., & Freudling, W. 1998, AJ, 116, 2632  
 Giovanelli, R., Haynes, M.P., Herter, T., Vogt, N.P., Da Costa, L.N., Freudling, W., Salzer, J.J., & Wegner, G. 1997, AJ, 113, 53  
 Guzman, R., & Lucey, J.R. 1993, MNRAS, 263, L47  
 Hill, R.J., et al. 1998, ApJ, 496, 648  
 Holtzman, J. A., et al. 1995, PASP, 107, 1065  
 Graham, J. A., et al. 1998, in preparation  
 Hudson, M. J. 1994, MNRAS, 266, 475

- Jerjen, H., & Tammann, G. A. 1997, *A&A*, 321, 713  
 Kennicutt, R.C., Jr., et al. 1998, *ApJ*, 498, 181  
 Kochanek, C.S. 1997, *ApJ*, 491, 13  
 Lucey, J.R., Currie, M.J., & Dickens, R.J. 1986a, *MNRAS*, 221, 453  
 Lucey, J.R., Currie, M.J., & Dickens, R.J. 1986b, *MNRAS*, 222, 427  
 Lucey, J.R. & Carter, D. 1988, *MNRAS*, 235, 1177L  
 Lynden-Bell, D., Faber, S. M., Burstein, D., Davies, R. L., Dressler, A., Terlevich, R. J., Wegner, G. 1988, *ApJ*, 326, 19L  
 Kelson, D. D., et al. 1996, *ApJ*, 463, 26  
 Macri, L. M., et al. 1999, astro-ph/9901332, preprint  
 Madore, B. F., & Freedman, W. L., 1991, *PASP*, 103, 933  
 Madore, B. F., et al. 1998, astro-ph/9812157, preprint  
 Musella, I. 1999, to appear in *Harmonizing Cosmic Distance Scales in a Post-Hipparcos Era* ed. D. Egret & A. Heck, astro-ph/9901043  
 Nevalainen, J., & Roos, M. 1998, *A&A*, submitted  
 Nusser, A., & Davis, M. 1995, *ApJ*, 421, 1  
 Pierce, M. J., Welch, D. L., McClure, R. D., van den Bergh, S., Racine, R., & Stetson, P. B. 1994, *Nature*, 371, 385  
 Press, W. H., Teukolsky, S. A., Vetterling, W. T., and Flannery, B. P. 1992, *Numerical Recipes in C*, 2nd ed. (New York: Cambridge University Press)  
 Rawson, D. M., et al. 1997, *ApJ*, 490, 517  
 Saha, A., Sandage, A., Labhardt, L. Tammann, G. A., Macchetto, F. D., & Panagia, N. 1997, *ApJ*, 486, 1  
 Sasselov, D. D., et al. 1997, *A&A*, 324, 471  
 Saunders, W., et al. 1998, in *Extragalactic Astronomy in the Infrared* ed. G.A. Mamon, Trinh Xuan Thuan, & J. Tran Thanh Van (Gif-sur-Yvette: Editions Frontieres)  
 Schechter, P.L., Mateo, M., & Saha, A. 1993, *PASP*, 105, 1342  
 Silbermann, N.A., et al. 1998, astro-ph/9806017, preprint  
 Stein, P., Jerjen, H., and Federspeil, M. 1997, *A&A*, 327, 952  
 Stellingwerf 1978, *ApJ*, 224, 953  
 Stetson, P. B. 1987, *PASP*, 99, 191  
 Stetson, P. B. 1996, *PASP*, 108, 851  
 Stetson, P. B., et al. 1998, *ApJ*, 508, 491  
 Tanvir, N.R. 1997, in *The Extragalactic Distance Scale*, ed. M. Livio, M. Donahue, & N. Panagia (Cambridge: Cambridge University Press), 91  
 Tonry, J. 1999, private communication  
 Willick, J.A. 1999, *ApJ*, submitted (astro-ph/9812470)  
 Willick, J.A., & Straus, M.A. 1995, *Physics Reports*, 261, 271  
 Willick, J.A., Courteau, S., Faber, S.M., Burstein, D., & Dekel, A. 1995, *ApJ*, 446, 12  
 Willick, J.A., Courteau, S., Faber, S.M., Burstein, D., Dekel, A., Strauss, M.A. 1997, *ApJS*, 109, 333  
 Yahil 1988, in *Large Scale Motions in the Universe*, ed. V. C. Rubin & G. V. Coyne (Princeton: Princeton University Press), 219  
 Zaritsky, D., Kennicutt, R. C. Jr., & Huchra, J. P. 1994, *ApJ*, 420, 87

TABLE 1  
 JOURNAL OF OBSERVATIONS

Mean Heliocentric Julian Date	UT Date	Filter	Exposure Time (s)
2450230.548	26 May 1996	F555W	7400
2450235.439	31 May 1996	F555W	7400
2450242.340	7 June 1996	F555W	7400
2450248.168	13 June 1996	F555W	7400
2450255.068	20 June 1996	F555W	7400
2450262.909	27 June 1996	F555W	7400
2450271.462	6 July 1996	F555W	7400
2450616.593	16 June 1997	F814W	7400
2450616.761	16 June 1997	F555W	4800
2450647.036	17 July 1997	F814W	7400
2450647.204	17 July 1997	F555W	4800

TABLE 2  
POSITIONS AND PROPERTIES OF CANDIDATE CEPHEIDS

ID	x (pix)	y (pix)	$\bar{V}$	$\bar{I}$	Amp.	$P$ (d)	$V$ prob.	$I$ prob.
37	476.14	68.22	27.45	26.03	0.68	30.00	0.75	0.12
71	502.61	74.47	27.35	26.20	1.02	28.00	0.98	0.88
200	139.98	98.63	27.46	26.55	0.89	54.00	0.81	0.32
304	489.95	126.40	27.36	26.45	0.74	32.00	0.85	0.83
307	520.29	126.66	27.32	26.53	0.62	33.00	0.69	0.68
342	108.36	134.79	27.51	25.66	0.67	59.00	0.30	0.50
391	132.02	146.45	27.01	26.42	0.73	28.00	0.55	0.91
445	330.47	155.53	27.65	26.33	0.85	46.00	0.74	0.79
500	186.48	169.34	27.96	26.69	0.75	30.00	0.88	0.87
526	52.90	176.19	27.01	26.32	0.61	35.00	0.68	0.84
722	576.78	230.69	27.24	27.20	0.62	39.00	0.78	0.01
747	632.36	240.76	27.52	26.52	0.66	48.00	0.53	0.31
774	406.08	245.75	27.43	26.46	0.73	24.00	0.53	0.33
780	155.82	247.20	27.26	26.39	0.64	52.00	0.72	0.41
871	543.66	264.40	27.29	25.97	0.73	48.00	0.88	0.84
982	404.30	290.64	28.00	26.57	0.79	39.00	0.72	0.87
1143	122.53	321.96	27.41	26.39	0.60	29.00	0.56	0.42
1165	710.62	325.30	27.24	26.53	0.64	60.00	0.60	0.12
1197	421.60	332.81	27.65	27.68	0.87	46.00	0.77	0.00
1211	53.49	335.78	27.19	25.59	0.61	36.00	0.73	0.01
1299	246.75	355.21	27.79	26.94	0.97	41.00	0.89	0.49
1326	191.60	362.40	27.52	26.41	0.79	28.00	0.86	0.71
1334	460.92	364.14	27.19	26.11	0.64	32.00	0.69	0.40
1392	261.67	382.01	27.57	26.72	0.90	24.00	0.86	0.86
1459	110.72	400.82	27.37	26.04	0.62	28.00	0.55	0.03
1490	197.25	410.22	27.19	26.39	0.71	35.00	0.87	0.88
1505	366.53	412.77	27.49	26.46	0.62	50.00	0.42	0.25
1538	186.76	424.29	27.55	26.12	0.66	45.00	0.56	0.59
1545	634.66	425.51	27.55	27.22	0.70	25.00	0.65	0.53
1639	608.91	445.56	27.64	25.74	0.66	57.00	0.18	0.44
1664	742.07	450.82	27.20	26.30	0.61	29.00	0.49	0.44
1672	450.42	453.07	27.50	26.07	0.68	31.00	0.75	0.20
1713	449.79	461.08	27.78	26.35	0.64	46.00	0.33	0.52
1724	454.95	462.87	27.41	25.67	0.75	41.00	0.87	0.29
1805	130.69	475.35	27.48	26.56	0.68	42.00	0.72	0.50
1991	447.24	506.10	27.48	26.33	0.65	36.00	0.72	0.62
2007	288.52	509.46	27.73	26.74	0.61	41.00	0.46	0.26
2035	429.14	512.80	27.39	25.25	0.97	28.00	0.97	0.00
2174	166.44	541.17	27.56	26.33	0.65	36.00	0.68	0.58
2177	80.42	542.45	27.56	27.68	0.62	50.00	0.34	0.00
2210	742.00	549.34	27.58	26.13	0.63	34.00	0.65	0.33
2333	571.57	571.99	27.58	26.55	0.60	60.00	0.19	0.09
2341	479.83	572.91	27.63	26.56	0.62	25.00	0.51	0.31
2497	420.90	599.54	27.72	25.59	0.70	44.00	0.50	0.20
2521	245.29	604.07	27.28	26.17	0.71	24.00	0.33	0.02
2547	271.99	608.05	27.57	27.23	0.79	26.00	0.81	0.61
2573	156.12	612.11	27.63	26.21	0.65	58.00	0.18	0.29
2625	176.03	621.03	27.39	26.27	0.76	25.00	0.66	0.18
2632	717.83	622.46	27.38	26.28	0.61	26.00	0.41	0.11
2697	391.70	633.54	27.26	25.91	0.62	44.00	0.77	0.59
2732	517.97	639.63	27.13	27.34	0.61	60.00	0.65	0.00
2774	284.92	646.25	26.78	25.24	0.67	32.00	0.56	0.00
2811	399.27	652.32	27.72	26.35	0.70	42.00	0.56	0.63
2848	353.40	657.40	26.90	26.56	0.89	59.00	1.00	0.38
2862	365.32	659.00	27.72	27.28	0.78	33.00	0.85	0.13
2958	757.54	673.55	27.28	27.25	0.72	26.00	0.57	0.59

TABLE 2—*Continued*

ID	x (pix)	y(pix)	$\bar{V}$	$\bar{I}$	Amp.	$P$ (d)	$V$ prob.	$I$ prob.
2968	613.42	676.07	27.60	26.74	0.66	35.00	0.69	0.48
2984	472.25	678.20	27.19	26.37	0.65	37.00	0.81	0.80
3130	474.75	713.00	27.63	26.64	0.65	56.00	0.18	0.06
3194	432.11	729.14	27.68	25.34	0.72	43.00	0.59	0.02
3237	187.01	739.28	27.93	26.53	0.83	48.00	0.46	0.72

TABLE 3  
OTHER DISTANCE ESTIMATES FOR NGC 4603 AND CEN30

Paper	Method	Number of Galaxies	$v_{Cen30, LG}$ ( $\text{km s}^{-1}$ )	$v_{4603}$ ( $\text{km s}^{-1}$ )	$v_{Cen30}$ ( $\text{km s}^{-1}$ )
Faber et al. 1989	$D_n - \sigma$	5	2802	...	$2221 \pm 208$
Lucey and Carter 1988	$D_n - \sigma$	15	2809	...	$3095 \pm 335$
Willick et al. 1997/EGAL	$D_n - \sigma$	22	2807	...	$2917 \pm 155$
Aaronson et al. 1989	Forward TF	10	2804	2740	$2830 \pm 248$
Willick et al. 1997/HMCL	Forward TF	10	3139	2759	$3445 \pm 213$
Willick et al. 1997/HMCL	Inverse TF	10	3139	2606	$3251 \pm 201$
Willick et al. 1997/MAT	Forward TF	5	3228	2599	$3000 \pm 273$
Willick et al. 1997/MAT	Inverse TF	5	3228	2443	$2881 \pm 262$
Giovanelli et al. 1998	Forward TF	39	2783	$2546 \pm 397$	$3012 \pm 98$
This Work	Cepheid	1	2807	$2395 \pm 306$	$\geq 2395 \pm 306$



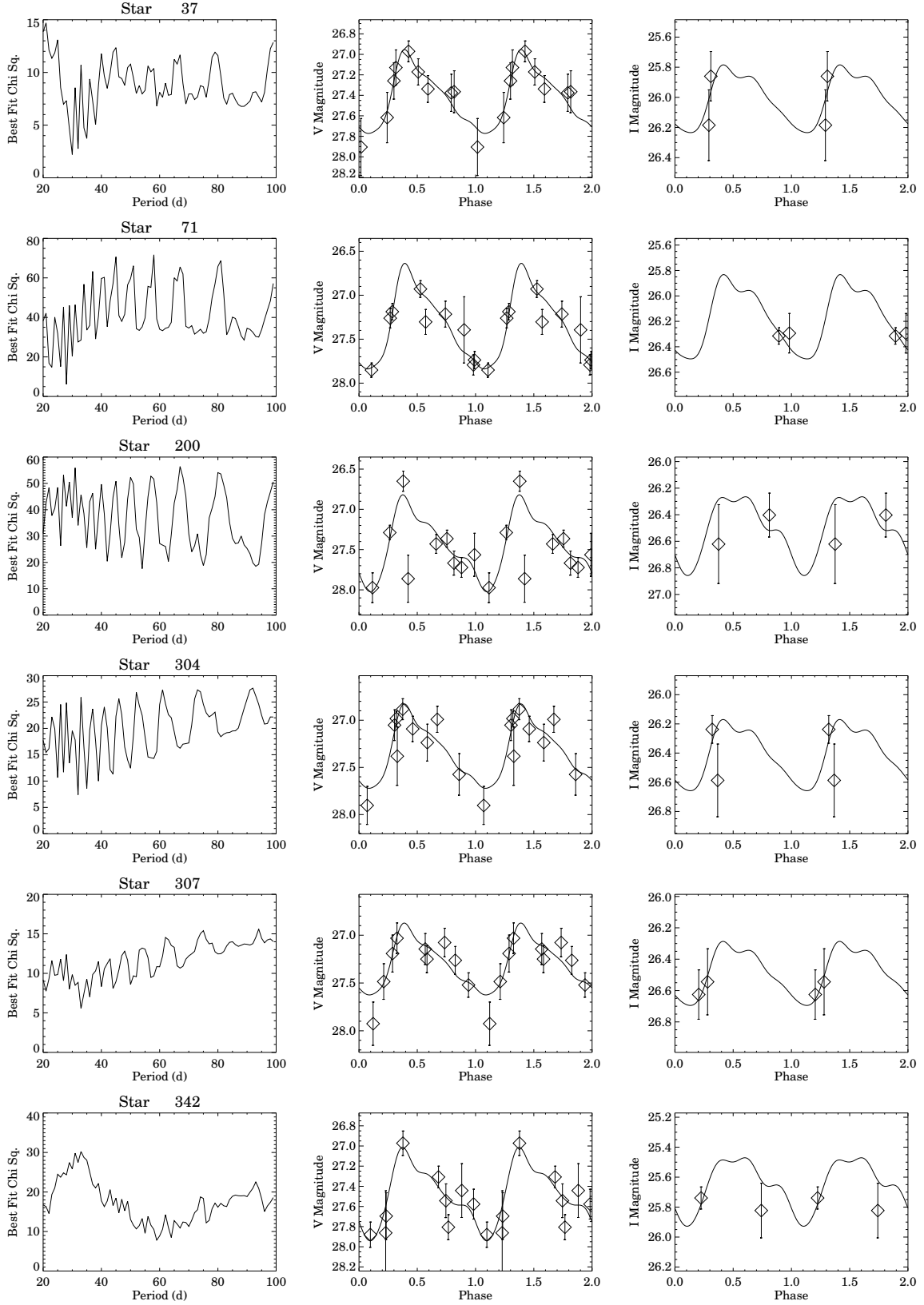


FIG. 10.— Light curves of a subset of our candidate Cepheids. In the leftmost panel for each star, the variation of  $\chi^2$  with period for fits to template Cepheid light curves is plotted; aliasing is readily apparent. In the center, the  $V$  magnitude for the candidate is plotted as a function of phase over two cycles, along with the best-fitting template light curve. The rightmost panel shows a similar plot for  $I$  magnitudes. Light curves for the entire sample may be obtained from our website.